Correspondence to:

D. H. Zhang,
zhangdh@pku.edu.cn

Revisiting the Variation of the Ionospheric Irregularities in the Low Latitude Region of China Based on Small Regional Geodetic GNSS Station Network

H. Y. Gao[1], D. H. Zhang[1] , Z. Z. Liu[2], S. J. Sun[3] , Y. Q. Hao[4] , and Z. Xiao[1]

[1]School of Earth and Space Sciences, Peking University, Beijing, China, [2]Department of Land Surveying and Geo-Informatics, The Hong Kong Polytechnic University, Hong Kong, China, [3]China Research Institute of Radio-wave Propagation, Qingdao, China, [4]School of Atmospheric Sciences, Sun Yat-sen University, Zhuhai, China

Abstract The rate of total electron content index (ROTI) and loss of lock (LoL) from global navigation satellite system (GNSS) observations are an important data source for ionospheric scintillation study. However, there are certain limitations of these data in ionospheric scintillation study, and clearing these limitations is important to understand the results from these data. In this paper, the variation of the ionospheric scintillation is revisited based on LoL and ROTI from a spatial dense GNSS network in the low latitude region of China. Via a priori knowledge of scintillation morphology, the method to determine the baseline ROTI for discriminating quiet and disturbed conditions is provided, and the abnormal data of ROTI and LoL unrelated to ionosphere are found and eliminated. Results show that the data examination is necessary. Using the qualified ROTI and LoL, the morphological variations of ionospheric irregularities are revisited. The temporal variation of ROTI and LoL are generally consistent, but there are some discrepancies. The maximum LoL occurrence is at about 21:00 LT, it is between 20:00 and 23:00 LT for ROTI. For spatial distribution, both parameters reach maximum occurrence in the southwest direction, but LoL is more concentrated. The azimuth range of maximum occurrence is 180–190° for LoL and 210–220° for ROTI. Statistically, the correlation between LoL occurrence and ROTI value from observation of single GNSS station is relatively good when ROTI <5 TECU/min, but it becomes worse when ROTI >5 TECU/min. However, their correlation can be greatly improved when data are averaged among all the stations.

Plain Language Summary The rate of total electron content index (ROTI) and loss of lock (LoL) from global navigation satellite system (GNSS) observations are an important data source for ionospheric scintillation study. However, there are certain limitations of these data in ionospheric scintillation study, and clearing these limitations is important to understand the results from these data. In this paper, the variation of the ionospheric scintillation is studied based on a small regional geodetic GNSS receiver network in Hong Kong, China. Via a priori knowledge of scintillation morphology, the baseline ROTI for discriminating quiet and disturbed conditions is determined. The morphological variations of ionospheric irregularities are studied. Results show that the temporal variation and spatial distribution of ROTI and LoL are generally consistent, but there are some discrepancies. Correlation between ROTI and LoL for large ROTI from single GNSS station is not good. However, it can be improved when data are averaged among all the stations.

1. Introduction

Ionospheric irregularities are plume-like structures in the ionosphere characterized by random fluctuation of ionospheric electron density. The main mechanism of ionospheric irregularity generation in the equatorial region is Rayleigh-Taylor instability, whose growth rate is modulated by regional parameters including electron density gradient, collision frequency, neutral wind and electric field (Abdu & Kherani., 2011; Sultan, 1996; Tsunoda, 1985). After their generation, the irregularities may rise under an upward $E \times B$ drift, and diffuse toward higher latitudes along magnetic field lines, forming a field-aligned elongated structure (Otsuka et al., 2002). As the generation of ionospheric irregularities is determined by multiple factors, the spatial and temporal distributions of the irregularities show considerable variation.

Radio signals propagating through these ionospheric irregularities undergo rapid amplitude and phase disturbance that is named as ionospheric scintillation (Aarons, 1977; Yeh & Liu, 1982). This phenomenon can bring about some adverse impacts on radio signal, for example, signal-to-noise ratio reduction, or in the most severe

Supervision: D. H. Zhang
Validation: H. Y. Gao, D. H. Zhang
Visualization: H. Y. Gao
Writing – original draft: H. Y. Gao
Writing – review & editing: H. Y. Gao, D. H. Zhang, Z. Z. Liu

conditions, signal blackout. The morphology of scintillation has been studied extensively via various types of ground-based instruments, for example, ionosondes and ionospheric scintillation monitor (ISM) developed from Global Navigation Satellite System (GNSS) receiver. Low-latitude region, as a high incidence area of scintillation (Kintner et al., 2007), has been the highlight of scintillation studies. These studies provide a basic understanding of the spatial and temporal distribution of ionospheric irregularities and scintillation.

Among all the types of ground-based equipment, the GNSS related receivers, due to its high availability and data continuity, has been one of the main data sources for the studies of ionospheric irregularities and scintillation in the past few decades. As early as 1980s, Basu and Basu (1981) proposed that the Global Positioning System (GPS) satellite, functioning as a satellite beacon, provides helpful information of the ionosphere. In 1993, the first ISM using the commercial GPS receiver was developed, from which the detailed temporal and spatial variation of the scintillation intensity can be obtained quantitatively (Van Dierendonck et al., 1993). Several parameters or indices have been proposed to quantify the intensity of ionospheric scintillation based on different aspects of the GNSS signal. The two standard and traditional scintillation indexes are S4, which is the standard deviation of normalized signal strength and reflects amplitude scintillation, and σ_φ, which is the standard deviation of detrended signal phase and reflects phase scintillation (Rino, 1979a, 1979b).

Besides S4 and σ_φ, some parameters that are derived from dual-frequency GNSS receivers can also be used to describe the condition of the ionospheric irregularities. In 1990s, the rate of change of TEC (ROT), that is the TEC difference of adjacent epochs divided by the sampling interval, was proposed to describe the strength of the ionospheric fluctuation (Aarons et al., 1996; Van Velthoven, 1990; Wanninger, 1993). Pi et al. (1997) further proposed the rate of TEC index (ROTI) that is the standard deviation of ROT over a 5-min interval to quantify the intensity of the ionospheric irregularities. Since then, the morphology of irregularities was studied mainly using ROTI index from single or regional GNSS receiver networks, among which includes the comparative evaluation studies between ROTI and other scintillation indexes (Basu et al., 1999; Olwendo et al., 2018; Yang & Liu, 2016). Although ROTI is less direct or precise than S4 and σ_φ in representing the condition of ionospheric irregularities or scintillation, these results show that it is a comparatively practical proxy index, with the extra advantage of better spatial coverage due to the higher availability of geodetic GNSS receivers than specialized scintillation receivers. Recently, ROTI Maps obtained from about 700 GPS stations located at high and middle latitudes of the Northern Hemisphere have been accepted officially by IGS as a new IGS ionospheric product characterizing the ionospheric irregularities occurrence (Cherniak et al., 2018).

Some abnormal tracking performances of GNSS receiver detected from GNSS observation, for example, cycle slip (CS) and loss of lock (LoL), were also widely used to reveal the distribution of ionospheric irregularities or scintillation. The CS or LoL is the temporary sudden skip of the integral carrier phase during carrier phase tracking performance of GNSS. The occurrence of CS or LoL with larger elevation is usually related to the effect of the ionospheric scintillation. Using CS data from GPS observations in the low latitude region of China, D. H. Zhang, Cai, et al. (2010) and D. H. Zhang, Xiao, et al. (2010) studied the characteristics of the GPS CS distribution and found that the CS occurrence shows the local time, seasonal and solar cycle variations that are similar to the morphology of ionospheric scintillation in China low latitude. Y. Liu et al. (2017) studied the temporal and spatial distribution of GNSS LoL occurrence during 2011–2015 using GNSS data near the southern side of the southern Equatorial Ionospheric Anomaly (EIA) in Asia-Oceania sector. Their results demonstrate the connection between the LoL and ionospheric scintillation through the spatial and temporal variation of LoL, as well as the dependence on the solar activity and geomagnetic activities. Similarly, with data from four GNSS stations located near southern EIA in American sector covering 24th solar cycle, Damaceno et al. (2020) investigated the relationship of LoL with local time, season, solar and geomagnetic activity. Their results indicate that the main features of LoL as a function of local and season strongly overlap with the scintillation climatology over Brazil. It should be noted that the CS and LoL are essentially the same phenomenon, distinguished by the duration relative to sampling rate, but CS detection is dependent on the detection method and the autocorrection algorithm of the receiver (Blewitt, 1990; Collin & Warnant, 1995), so unlike LoL, the CS occurrence rates derived from the same data source by different CS detection methods may be different.

The aforementioned GNSS receiver-based scintillation-related parameters (S4, σ_φ, ROT, ROTI, CS, and LoL) have greatly enriched ionospheric scintillation data source, and the studies based on these parameters have greatly deepened our understanding of ionospheric irregularities and scintillation. However, although all these parameters are related to scintillation and generally correlated to each other, each of them reflects different aspect of the

ionospheric scintillation effect on radio signal or system, so discrepancy among different parameters is expected in certain conditions. Basu et al. (1999) compared the ROTI and S4 index observed in Ascension Island. They considered that the ROTI can be used to predict the presence of scintillation in some condition, but the quantitative relationship between ROTI and S4 varies considerably due to variations of the ionospheric projection of the satellite velocity and the ionospheric irregularity drift. According to the theory about the angle dependence of scattered of radio-wave in anisotropic medium (Rino & Fremouw, 1977), Carrano et al. (2019) presented a quantitative theory for the ROTI by noting its relationship to the phase structure function of ionospheric turbulence, with which the dependence of ROTI on the sampling interval, satellite motion, propagation geometry, and the spectral shape, strength, anisotropy, and drift of the irregularities was provided. It is clearly put forwards that the ratio of ROTI to S4 depends on the particular viewing geometry for each satellite represented by the relative velocity between the ionospheric penetration point (IPP) and the drifting irregularities. Obviously, this dependence will increase the variability of the ROTI in indicating the ionospheric irregularities based on the traditional dual-frequency GNSS data. More recently, by comparing S4 from scintillation receivers and ROTI from nearby geodetic receivers in China low latitude, Li et al. (2022) summarized the limitations of ROTI in indicating ionospheric scintillation and quantitatively evaluated the reliability of ROTI in monitoring ionospheric scintillation.

In general, the following aspects did not receive enough attention in the previous studies with these scintillation-related parameters. Obviously, the value of ROTI is related to the sampling rate of TEC and the time interval of standard deviation calculation (Jacobsen, 2014). In the early studies, the TEC used in ROTI calculation are mainly calculated from GPS measurements with 30-s sampling rate, and the threshold of ROTI related to ionospheric irregularities was set to be 0.5 TECU/min (Pi et al., 1997). With the progress of hardware and signal processing technology, the low-noise receiver with high sampling rate output have been developed and used widely. In addition, the sampling rate of GNSS data is occasionally different, the ROTI derived from different sampling rate should reveal the ionospheric irregularities with different scale (Basu et al., 1999). In the past, the examination or the determination of the threshold value of scintillation related ROTI was seldom done. There is no universally accepted baseline value to separate the quiet and disturbed conditions, and it is impossible to delimit a uniform threshold for ROTI from different data sources. There was limited such work of quantifying ionospheric scintillation focused on ROTI thresholds with different sample rate of GNSS data in previous studies (Jacobsen, 2014; Li et al., 2022). In this paper, we will provide a method to determine ROTI threshold based on a priori knowledge of the variation of the ionospheric scintillation and irregularities.

The second aspect is the individual difference of GNSS receivers. Although the LoL behaves similar variation pattern with that of S4 or phase scintillation index in temporal and spatial scale, it should be noted that LoL is the event of GNSS abnormal performance that depends not only on the ionospheric scintillation but also on the signal tracking ability and quality of individual GNSS receivers. Without cautious data examination process, the LoL abnormal events due to hardware or receiver performing failures may be determined as an event related to ionospheric condition, so the quantitative comparison of LoL occurrence among different data sources should be careful. Chen et al. (2005) studied the LoL distribution for 10 types of GPS receiver during the same time interval of the great solar flare on 28 October 2003, they found that the LoL events are dependent on receiver type and receiver tracking mode. D. H. Zhang, Xiao, et al. (2010) studied the CS occurrence based on the GPS data from six same type GPS receivers near EIA region in China, their results found that for the GPS data from two receivers apart about 50 km, the CS number in the same time interval is very different although their variation tendency with local time and seasons are similar. Through the analysis of the LoL event of GPS receiver with different bandwidth of phase-locked loop (PLL) in Swarm satellites, Xiong et al. (2018) found that some GPS signal loss events are not related to the ionospheric plasma irregularities occur when the PLL bandwidth increased lager than 0.5 Hz. Using data in 2015 from 13 GNSS receivers distributed globally, Z. Liu et al. (2019) made a more extensive research on the difference of ROTI by GNSS system, signal combination and receiver types. They found that the average ROTI from certain receivers and signal combinations can be more than four times larger than others. Although the influence of the individual difference among receivers has been widely known, previous studies generally seldom concern this problem properly when applying GNSS-based data to morphological or case studies.

There are 14 dual-frequency geodetic GNSS receivers affiliated to the Hong Kong Satellite Positioning Reference Station Network (SatRef) in Hong Kong region that are located in a small region less than 0.5° apart in geographic longitude and latitude in China low latitude. Different with the traditional IGS GNSS data, the sample rate of the SatRef receiver in routine observation is 5-s. As Jacobsen (2014) noted that a sizable amount
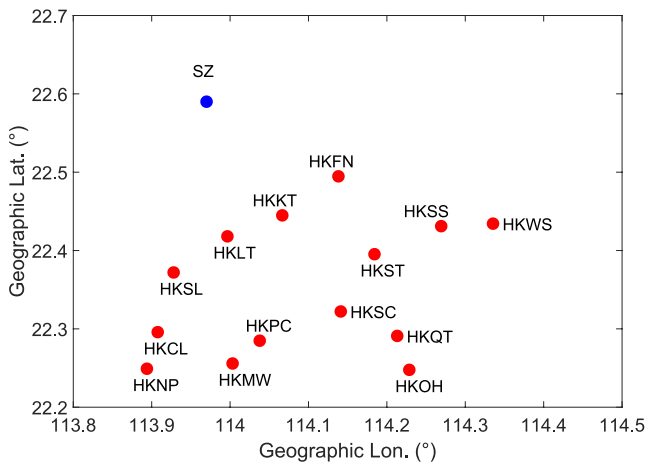
Figure 1. Geographic locations of the stations used in this study, including 14 geodetic global navigation satellite system receivers (red circles), and a Global Positioning System Ionospheric Scintillation Monitor (blue circle).

of data must be analyzed to determine a suitable baseline for delineating quiet and disturbed conditions, this dense distributed and high sample rate GNSS network provides an advantage for revealing the problems concerning ROTI and LoL data derived from traditional dual-frequency GNSS receivers. In this study, following aspects will be focused on based on this GNSS network. First, the method to determine ROTI threshold for discriminating quiet and disturbed conditions will be proposed according to the prior knowledge about the variation of ionospheric scintillation in this region (D. H. Zhang, Cai, et al., 2010; M. Zhang et al., 2019). Then, examples of how to detect false scintillation events in LoL and ROTI derived from GNSS observation by cross test are given. Finally, the variation of ionospheric irregularities represented by LoL and ROTI parameter, the correlation and the discrepancy between LoL and ROTI will be given based on these examined data.

2. Data and Methodology

The data used in this study are from 14 dual-frequency geodetic GNSS receivers affiliated to SatRef network from 2012 to 2016. The sample rate of the GNSS observations in SatRef is 5 s. From the observations of these receivers, the scintillation-related parameters ROTI and LoL can be obtained. Besides, the S4 index data from the ISM receiver at Shenzhen (SZ) station (22.59°N, 113.97°E) are also used, which belongs to the Chinese Meridian Project network. Figure 1 gives the geographic distribution of the receivers used in this study. The geographic longitude, geographic latitude, receiver type and data availability for each SatRef receiver is presented in Table 1. Data availability is generally high (>95%) for most of the stations and most of the years, except for HKFN in 2015 and 2016, HKMW in 2015. The type of ISM at SZ station (not shown in the table), is GSV4004B. The sample rate of the S4 is 1 min.

ROTI is the main proxy of ionospheric irregularities in this study. To compute ROTI, the slant total electron contents are calculated for every receiver–satellite tracking arc epoch by combining the pseudo-range and carrier phase observations in two L-band carrier signals, $f_{L1} = 1.5754$ GHz and $f_{L2} = 1.2276$ GHz. ROT is calculated by the following formula:

$$\text{ROT} = \frac{\text{sTEC}(t + \Delta t) - \text{sTEC}(t)}{\Delta t} \tag{1}$$

where Δt is the time resolution of the observation data, which is 5 s in this study. It should be noted that the sample rate of the raw GNSS data is 5 s, the ROT with different sampling time interval, for example, 5–30 s, can be calculated that represents the ionospheric irregularities of different scale sizes (Basu et al., 1999). Here, 5-s of sampling rate is selected to represent the smallest irregularities that the SatRef network can provide. For details about the TEC calculation, see D. H. Zhang, Zhang, et al. (2010). ROTI is defined as the standard deviation of ROT over 5 min:

$$\text{ROTI} = \sqrt{\langle \text{ROT}^2 \rangle - \langle \text{ROT} \rangle^2} \tag{2}$$

This result is considered the ROTI value of the midpoint of the 5-min interval. Then, ROTI is calculated by moving epoch by epoch (5 s) with 5-min interval for each continuous receiver-satellite tracking arc. To restrain the possible multipath effect, the cutoff angle of the satellite elevation is set to be 30°. The obtained ROTI value is projected to the ionospheric pierce point (IPP), the intersection between the receiver-satellite line of sight and the ionospheric thin shell, which is assumed to be 400 km in height.

To determine the effect of ionospheric irregularities on GNSS signal tracking ability, the LoL data in L1 and L2 band signals are collected from the carrier phase measurement in raw GNSS data, respectively. The LoL occurrence expressed as percentage (LoL%) is computed as:

$$\text{LoL\%} = \frac{N_l}{N_t} \times 100\% \tag{3}$$

Table 1
The Geographic Coordinates, Receiver Types, and Data Availability of the 14 SatRef Stations

	Geographic longitude	Geographic latitude	Receiver type	Data availability by year (days/percentage)				
				2012	2013	2014	2015	2016
HKCL	113.9077	22.2958	Trimble NetR9	365/99.73	343/93.97	365/100.00	365/100.00	366/100.00
HKFN	114.1382	22.4947	Leica GRX1200	366/100.00	354/96.99	365/100.00	62/16.99	136/37.16
HKKT	114.0666	22.4449	Leica GRX1200	366/100.00	354/96.99	365/100.00	364/99.73	366/100.00
HKLT	113.9966	22.4181	Leica GRX1200	365/99.73	354/96.99	365/100.00	365/100.00	366/100.00
HKMW	114.0032	22.2558	Leica GRX1200	366/100.00	354/96.99	362/99.18	301/82.47	366/100.00
HKNP	113.8939	22.2491	Leica GRX1200	366/100.00	354/96.99	365/100.00	365/100.00	365/99.73
HKOH	114.2286	22.2477	Leica GRX1200	366/100.00	354/96.99	365/100.00	365/100.00	365/99.73
HKPC	114.0378	22.2849	Leica GRX1200	364/99.45	354/96.99	365/100.00	364/99.73	366/100.00
HKQT	114.2132	22.2910	Trimble NetR9	356/97.27	354/96.99	363/99.45	364/99.73	359/98.09
HKSC	114.1412	22.3222	Leica GRX1200	366/100.00	353/96.71	365/100.00	365/100.00	365/99.73
HKSL	113.9280	22.3720	Leica GRX1200	366/100.00	354/96.99	364/99.73	365/100.00	366/100.00
HKSS	114.2693	22.4311	Leica GRX1200	366/100.00	354/96.99	365/100.00	363/99.45	365/99.73
HKST	114.1842	22.3953	Leica GRX1200	366/100.00	354/96.99	365/100.00	365/100.00	365/99.73
HKWS	114.3354	22.4343	Leica GRX1200	366/100.00	354/96.99	365/100.00	365/100.00	366/100.00

where N_t is the total number of theoretically observable epochs (5 s) calculated from the ephemeris files for certain time period, and N_l is the total number of LoL event for the same time period (i.e., number of epochs not recorded in the observation files). Same with ROTI, a cutoff angle of 30° is also applied to the LoL collection. By the way, L2 has a lower signal-to-noise ratio and is more susceptible to scintillation, thus statistically, for the same ionospheric irregularities condition, LoL in L2 occurs more often than that in L1, or LoL in L1 corresponds to more intense irregularities condition. In order to investigate the discrepancies between the LoL events in L1 and in L2 with different degrees of severity, LoL occurrences in L1 and L2 are calculated separately. Also, to show the temporal and spatial distribution of the LoL occurrence, the time and location information is also recorded in LoL extracting process.

3. Results

3.1. Evaluation of ROTI and LoL

The ROTI is the standard deviation of the standard TEC variation. Besides the ionospheric irregularities, its value is influenced by some other factors, such as the receiver performing condition, the thermal noise of the receiver hardware, and the background ionospheric fluctuation. So, there should be a limitation or threshold so that only the ROTI larger than this threshold value is related to the ionospheric irregularities. In addition, it is found that, even at high elevation angles, some LoL events or larger ROTIs may be unrelated to ionospheric irregularities. These kinds of abnormal events should be eliminated from the data source for irregularities study. The ionospheric irregularities condition over small regional distributed GNSS stations is very similar. Therefore, the ROTI or LoL data related to the ionospheric scintillation obtained from the data of different GNSS stations in the same time interval should be consistent. Through the cross-comparison of these data and a prior temporal variation of the ionospheric scintillation or irregularities in this region, the ROTI threshold for the ionospheric irregularities can be obtained, also the abnormal data unrelated to the ionospheric irregularities can be determined and removed. In this section, based on the small regional multi-station GNSS network, we will provide a method to determine the ROTI threshold and provide examples to extract abnormal LoL event or large ROTI that is not caused by ionospheric irregularities.

3.1.1. Determining the ROTI Threshold

Due to the background fluctuation of ionospheric plasma density, there is a baseline level of ROTI for discriminating quiet and disturbed conditions. The least ROTI value related to irregularities, or the ROTI threshold, is to be determined in this section. The ROTI threshold depends on the sampling rate of TEC (as is mentioned above), as well as the hardware noise of the receiver and observation condition. Note that Pi et al. (1997) used 30-s TEC data with a ROTI threshold of 0.5 TECU/min, and that their data were chosen during solar minimum (1993–1997). With the development of GNSS technique, GNSS receivers with high sampling rate and lower hardware noise are used in many GNSS applying fields. Obviously, the evaluation of the ROTI threshold value is useful for the related ionospheric scintillation and irregularities studies with ROTI data.

The ROTI threshold which corresponds to irregularities can be determined through the diurnal or seasonal distribution of ROTI values according to
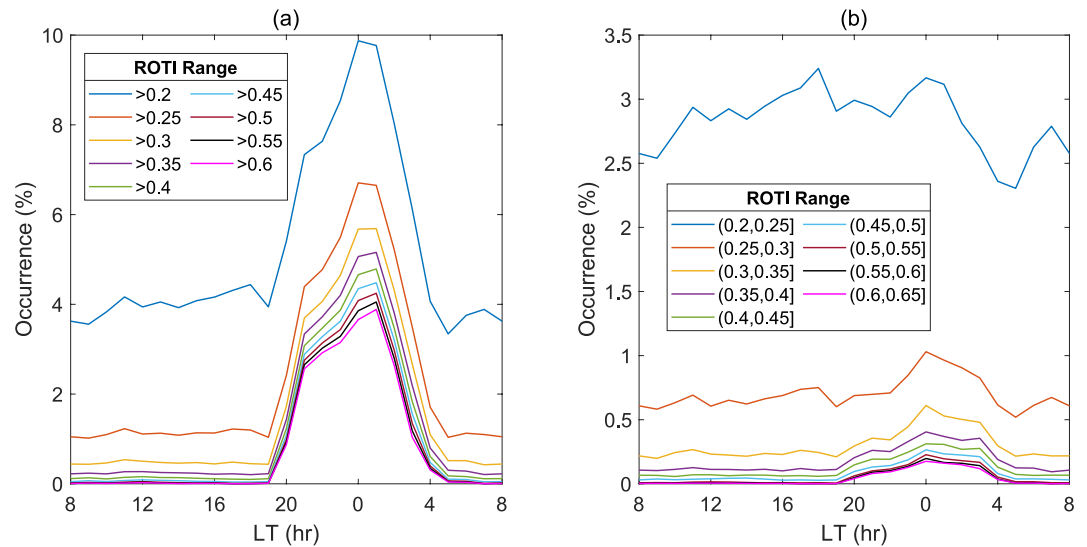
Figure 2. Local time variation of the proportion that ROTI falls within given ranges, averaged over 5 years (2012–2016) and 13 stations (excluding HKCL). Unit of ROTI is TECU/min. Each colored line in each panel represents one ROTI range. For example, the blue line in (a) indicates the local time variation of the proportion of ROTI that is greater than 0.2 TECU/min in the total ROTI data.

a priori knowledge about the temporal variation of the ionospheric irregularities or scintillation. According to the local time variation of the ionospheric irregularities, the irregularities-induced component mainly occurs from sunset to near midnight, while the background component that is not related to irregularities shall not have significant this local time variation. Using data from 2012 to 2016 of the 13 stations (excluding HKCL, the reason will be given later), Figure 2 presents the diurnal variation of the proportion of the ROTI under different trial thresholds ranging from 0.2 to 0.6 TECU/min, with a step size of 0.05 TECU/min. Figure 2a shows that for different ROTI thresholds, the irregularities occurrence, defined as the proportion of ROTI greater than the given threshold, is always higher at night (18:00–04:00 LT) than that during the daytime period. To better distinguish the background and irregularities components, the local time variation of the differences between the percentages of adjacent ROTI ranges in Figure 2a are calculated and presented in Figure 2b. The (0.2, 0.25] TECU/min component presents less local time variation, so it belongs to the background. The (0.25, 0.3], (0.3, 0.35], and (0.35, 0.4] TECU/min components show some daily variation, but the daytime values are still relatively high, so these values of ROTI still include a large proportion of the background components. The (0.4, 0.45] TECU/min and (0.45, 0.5] TECU/min components are very weak during the daytime, so 0.4 or 0.45 TECU/min can be chosen as a threshold to demarcate the weak irregularities and ionospheric background condition.

Apart from local time distribution, the seasonal distribution of ionospheric irregularities is also capable of determining the ROTI threshold. Figure 3 gives the normalized number distribution of ROTI value from all 13 stations (a) and from HKWS station (b) during the period from 2012 to 2016. Because the irregularities occurrence exhibits seasonal variation, this number distribution given in Figure 3 is classified as spring months (Mar and Apr), summer months (Jun and Jul), and autumn months (Sep and Oct). It is obtained through accumulating the number of data points whose ROTI falls in the given range (from 0.00 to 7.00 TECU/min, step size 0.05 TECU/min) divided by the total number of data points within each months' period. The proper ROTI threshold for irregularities condition can be easily determined from this figure. It can be seen that the ROTI distributions for the value less than 0.3 in different seasonal months are very similar, which should demonstrate the fluctuation of the ionospheric background condition. The distributions of ROTI in different seasonal group gradually separate when the ROTI larger than 0.4 TECU/min. When ROTI is sufficiently large (>0.45 TECU/min, as shown in the dashed lines), the normalized frequency in spring months (Mar and Apr) always stays above the autumn months (September and October) and the autumn months above the summer months (June and July). The threshold ROTI value derived from seasonal variation is thus 0.4 or 0.45 TECU/min, which is consistent with the value determined by diurnal distribution. This method can also be used for the data from a single station. Figure 3b shows the normalized number distribution of ROTI value obtained from observations at HKWS station from 2012 to 2016.
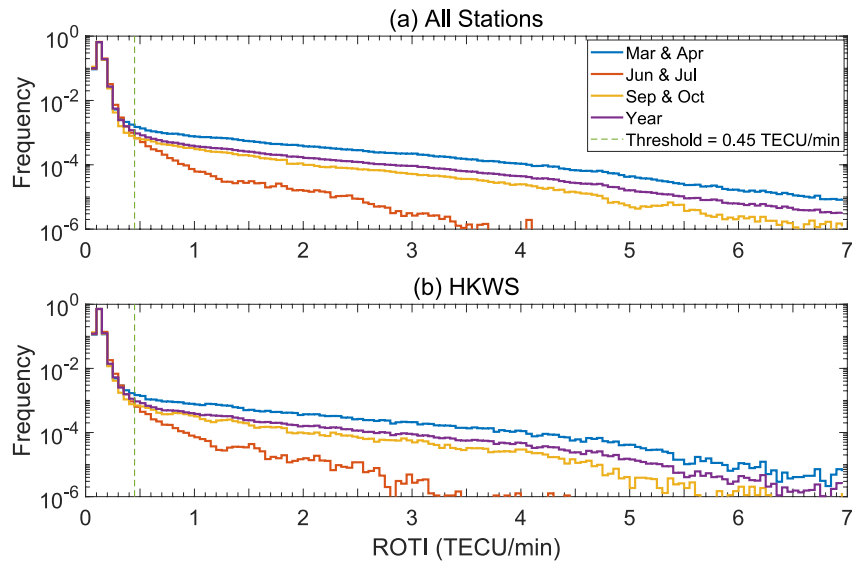
Figure 3. Normalized number distribution of ROTI data in different ROTI range of three seasonal periods, averaged over 5 years (2012–2016), from 13 stations (a) (excluding HKCL), and HKWS (b). "Frequency" refers to the accumulated number of data points whose ROTI falls in the given range (from 0.00 to 7.00 TECU/min, step size 0.05 TECU/min) divided by the total number of data points in certain months period.

It can be seen that the distributions are very similar with the results of multiple stations, although the curves are not smooth for large ROTI values. To ensure that the background being cleaned up, the ROTI threshold in this study is set as 0.5 TECU/min, that is, irregularities is considered to be present when ROTI >0.5 TECU/min. Note again that the threshold of ROTI is related to the sample rate of TEC, so the value 0.5 TECU/min is derived only from the data with 5-s sampling rate and is not universally applicable. We also exam the threshold for the ROTI calculated with 30-s sampling rate, it is found the ROTI threshold for 30-s sampling rate is about 0.25 TECU/min (not given here). In addition, it should be noted that this method is only effective when the amount of data and their time coverage are statistically large, because scintillation or irregularities in the daytime and summer, albeit rare, is possible.

3.1.2. Detection of Abnormal LoL and ROTI Not Related to Ionospheric Irregularities

Enhancement of irregularities-related parameters may be occasionally caused by abnormal status of receivers or satellites. This kind of enhancement is not related to the ionospheric scintillation or irregularities and should be removed. In practice, data cross checking is a useful method for data quality examination through analyzing data from different receivers. Figure 4a gives the local time distribution of LoL occurrence from five receivers in 2013. It can be seen that the local time distribution of LoL occurrence from HKFN, HKLT, HKMW, and HKOH stations coincide well. LoL mainly occurs between 19:00 LT and 24:00 LT that is roughly agreed with the local time distribution of low latitude ionospheric irregularities. However, the LoL occurrence from HKCL is obviously larger than that from other stations, and its local time variation is also very different from that of other stations. According to a priori knowledge of this region, the ionospheric irregularities in the low latitude mainly occur after sunset and seldom occurs in the daytime (Aarons, 1982). Obviously, these LoL events occurred in HKCL receiver are not related to ionospheric irregularities. To further validate the abnormal LoL data in HKCL, the variation of the IPP latitude of LoL events with local time is presented in Figure 4b. As a comparison, the result from HKFN is also given in Figure 4c. It can be seen that the LoL event from HKFN mainly occurs from sunset to midnight period and in limited low latitude region, while for HKCL, LoL event occurs frequently in observation latitude range, which reflects obvious tracking curves of some GPS satellites. This indicates that there were frequent continuous LoL incidents lasting hours at HKCL station. Similar abnormal LoL distribution also occasionally happens in HKQT station. These continuous LoL events should be related to the performing status of the GNSS receiver and are not caused by ionospheric irregularities, hence the LoL data from HKCL and HKQT are excluded in the following studies.
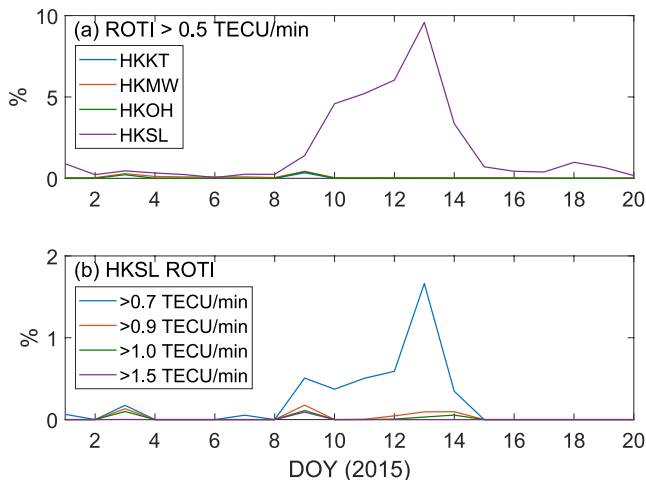
The LoL and ROTI data from nearby receivers should exhibit consistent variations, but it is found that there are some exceptional values on individual days for some receivers occasionally. For example, on DOY 351 in 2014,
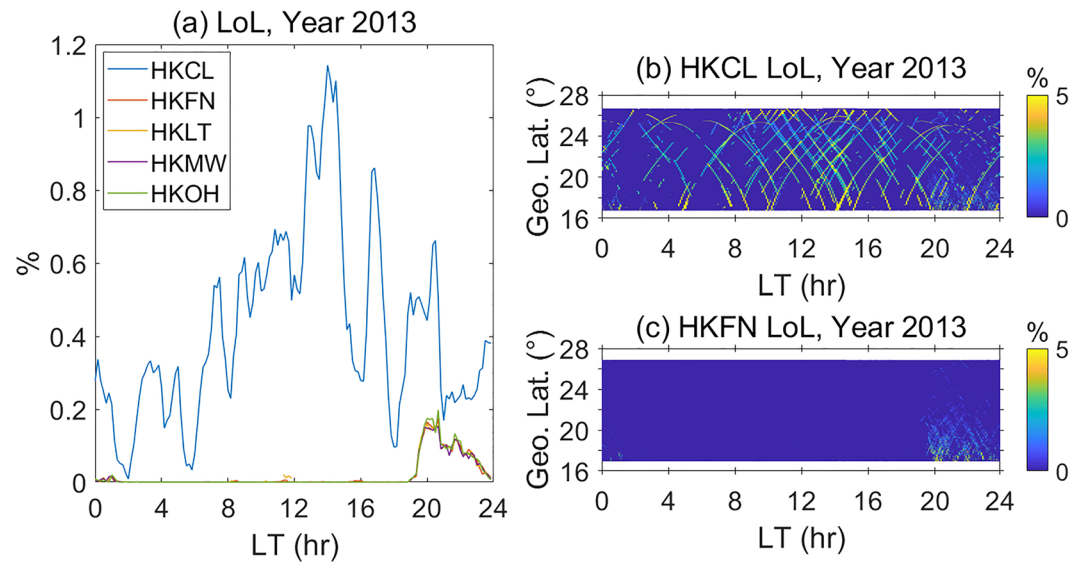
Figure 4. (a) Local time distribution of loss of lock (LoL) occurrence in L2 from HKCL, HKFN, HKLT, HKMW and HKOH in 2013. (b) Local time and geographic latitude distribution of LoL occurrence in L2 from HKCL in 2013. (c) Local time and geographic latitude distribution of LoL occurrence in L2 from HKFN in 2013.

the LoL of L2 from the station HKFN is significantly higher than the other stations, reaching 4.36%, while the LoL occurrence of the other stations in December 2014 is generally under 0.01%. We analyzed the season-PRN distribution of LoL of L2 in 2014 from HKFN (figure not given), and found that on DOY 351, the LoL occurrence for satellite PRN 2 in HKFN is as high as 87.6%. According to the data of the other stations, this can be judged as an abnormal event which may be associated with channel abnormality of the receiver. These abnormal LoL events should be eliminated in scintillation or irregularities analysis also.

Similar abnormalities can also be found in ROTI data. In the study of the monthly variation of ROTI derived from different GNSS receiver, the occurrence of ROTI >0.5 TECU/min in January 2015 is obviously larger than that from other stations. In order to check the reason, the occurrence of the ROTI larger than 0.5 TECU/min from four station during the first 20 days of 2015 is given in Figure 5a, it can be seen that the percentage occurrence of ROTI >0.5 TECU/min from HKSL is much higher than that in other stations during the period from DOY 9 to DOY 15. To further analyze these abnormal ROTI data, the occurrence of ROTI from HKSL under different thresholds (0.7, 0.9, 1.0 and 1.5 TECU/min) in the first 20 days of 2015 is shown in Figure 5b. It appears that a threshold of 0.9 TECU/min is enough to eliminate the high ROTI occurrence on DOYs 10–14, so we think that this event should not be simply classified as receiver failure. It is probably caused by the occasional large phase observation noise of the receiver or the observation environment interference that is out of the scope of this study. By the way, the abnormal ROTI event like above also occurs in HKSC station in September 2015. On the whole, although the threshold of 0.5 TECU/min is good when taking all the data into consideration, it may be occasionally improper for a certain receiver on a certain day and these abnormal ROTI data should be removed also.

3.2. Morphology

3.2.1. Diurnal, Monthly Variation of ROTI and LoL

Through the data quality verification mentioned above and eliminating the abnormal data, the morphological variation of the ionospheric irregularities in China low latitude can be revealed with qualified LoL and ROTI parameters. Figure 6 gives the monthly variation of the occurrence of LoL (L1 and L2) and ROTI (threshold 0.5 TECU/min) from 12 stations. The data of
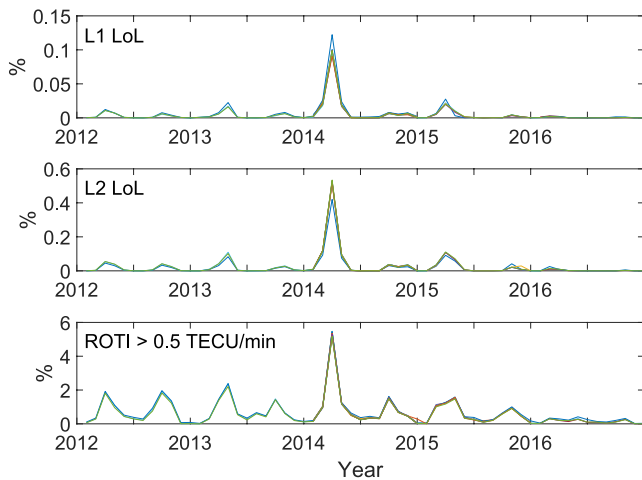

Figure 5. (a) The proportion of ROTI that exceeds 0.5 TECU/min in each day of the first 20 days of year 2015, observed from HKKT, HKMW, HKOH and HKSL. (b) The proportion of ROTI that exceeds different thresholds (0.7, 0.9, 1.0 and 1.5 TECU/min) in each day of the first 20 days of year 2015 observed at HKSL.

Figure 6. Monthly variations of (top) loss of lock (LoL) occurrence in L1, (middle) LoL occurrence in L2 and (bottom) the occurrence of ROTI >0.5 TECU/min. Each colored line represents data from one receiver, total 12 receivers.

each station were calculated separately, and averaged over 1-month intervals. By comparison among the panels, it can be seen that LoL occurrences exhibit a similar trend as ROTI, with higher values near equinox months, forming two peaks at spring and autumn every year. LoL and irregularities events (ROTI >0.5 TECU/min) reach peak occurrence in April 2014 (LoL peak occurrence rate in L1, L2, and ROTI is larger than 0.1%, 0.4% and 5%, respectively), while the lowest occurrence appears in 2016. This year-to-year variation pattern is basically correlated with solar activity. Besides the peak occurrence near equinox months, the ROTI >0.5 TECU/min also occurred in other months in some years, for example, in 2013 and 2014 summer that not obviously occurs in LoL in L1 and L2. Since the loss of carrier signal usually occurs during intense ionospheric scintillation or irregularities conditions, this difference can be understood. Furthermore, we notice that during the time range of our observation, although the occurrence rate maxima of all the parameters fall on equinox months (March and September), scintillation is always more frequent in vernal months than in autumnal months every year. We know that the ionospheric fluctuation is positively correlated with the background TEC along the signal propagation path, which is one of the main reasons why the low-latitude ionospheric scintillation amplitude is positively correlated with solar activity. Figure 7 gives the monthly variation of ionospheric vertical TEC at 12:00 LT and 21:00 LT from HKWS during 2012–2016, which shows that at 21:00 LT, the vertical TEC in spring months is greater than that in autumn months every year. This indicates that the monthly variation of ionospheric irregularities may be partly related to the background TEC.

Figure 8 shows the local time distribution of the LoL occurrence rate of L1 and L2 and ROTI in 2014 from 12 stations based on the qualified data. ROTI is classified into three levels (>0.5, 1, and 2 TECU/min) to represent three levels of irregularities intensity. It appears that both LoL and ROTI occur at night from about 19:00 LT to about 3:00 LT (20:00 LT–01:00 LT for LoL, and 19:00 LT -03:00 LT for ROTI), and the local time distribution of same parameter among different stations is very consistent. Nevertheless, there are some obvious differences between the local time distribution of LoL and ROTI with different class. LoL occurrence increases abruptly after 20:00 LT, reaches the maximum at 21:00 LT, decreases quickly afterward, and rarely occurs after midnight. ROTI occurrence rate mainly increases during 19:00–01:00 LT, and changes smoothly during 20:00-00:00 LT. The peak time of ROTI >0.5 TECU/min and >1 TECU/min is at midnight, it is 21:00 LT for ROTI >2.0 TECU/min. Comparatively, the occurrence rate of ROTI >2 TECU/min seems more consistent with that of LoL. This local time difference between the ROTI and LoL will be discussed in discussion section.

Similarly, we can average all the data from different stations in this area to reveal the local time distribution of LoL and ROTI caused by ionospheric irregularities in different years comprehensively. Figure 9 shows the variation of occurrence rate of LoL and classified ROTIs on local time, averaged over one-hour intervals and over all 12 stations from 2012 to 2016. Results from different years are shown in separate panels. As for year-to-year variation, the distribution of LoL and ROTI is similar to Figure 6, with the peak occurrence in 2014. However,

the year-to-year variation of ROTI is less significant than LoL, and this is somewhat different from the monthly variation in Figure 6. It is noted that in some other months there is also large ROTI but hardly in LoL, and this should contribute to the relative insignificance of the year-to-year variation of ROTI. As is shown in the figure, LoL and ROTI follow a similar variation pattern with local time, with higher values between 19:00 and 02:00 LT. Same to Figure 8, three levels are chosen for ROTI. Although the trends are similar for different ROTI thresholds, the local times when ROTI occurrence rate reaches the peak are a little different. For level of ROTI >0.5 TECU/min, the peak occurs at 21:00 in 2015, at 22:00 in 2012, at 23:00 in 2013 and 2016, at 00:00 in 2014. For level of ROTI >1 TECU/min, the peak occurs at 22:00 in 2012, at 00:00 in 2014, at 21:00 in the other years. For ROTI >2 TECU/min, the peak occurs at 22:00 in 2014, at 21:00 in the other years. Comparing the local
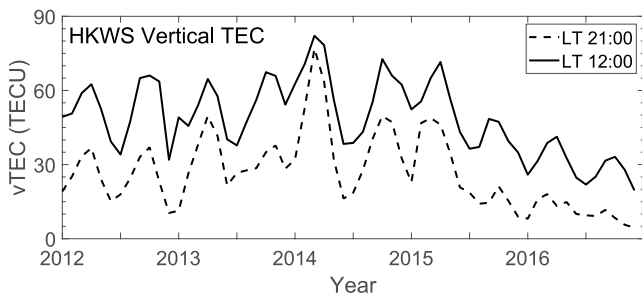
Figure 7. Monthly variations of vertical TEC from HKWS station. Dashed (solid) line represents vertical TEC at local time 21:00 (12:00).
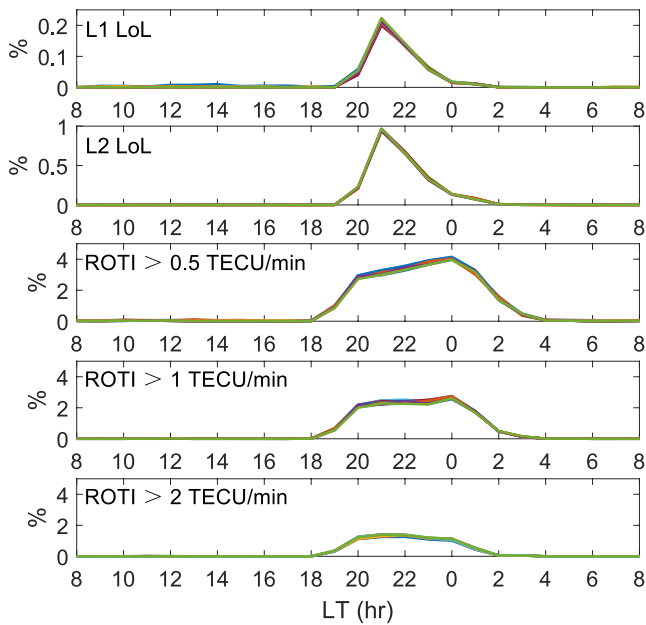
Figure 8. Local time variations of loss of lock occurrence in L1, L2, and the occurrence of ROTI with three levels in 2014 from 12 stations. Each colored line represents data from one station.

time of peaks with that in LoL panels, it can be concluded that the level of ROTI >2 TECU/min matches LoL better than the other two levels. It can also see that the LoL occurrence rate of L2 is approximately 4 times as that of L1 that represents the different anti-interference ability of the two carrier signals related to their signal configuration (Kintner et al., 2007; D. H. Zhang, Cai, et al., 2010). This difference of the LoL in L1 and L2 can be used to represent the different intensities of the ionospheric irregularities or scintillation.
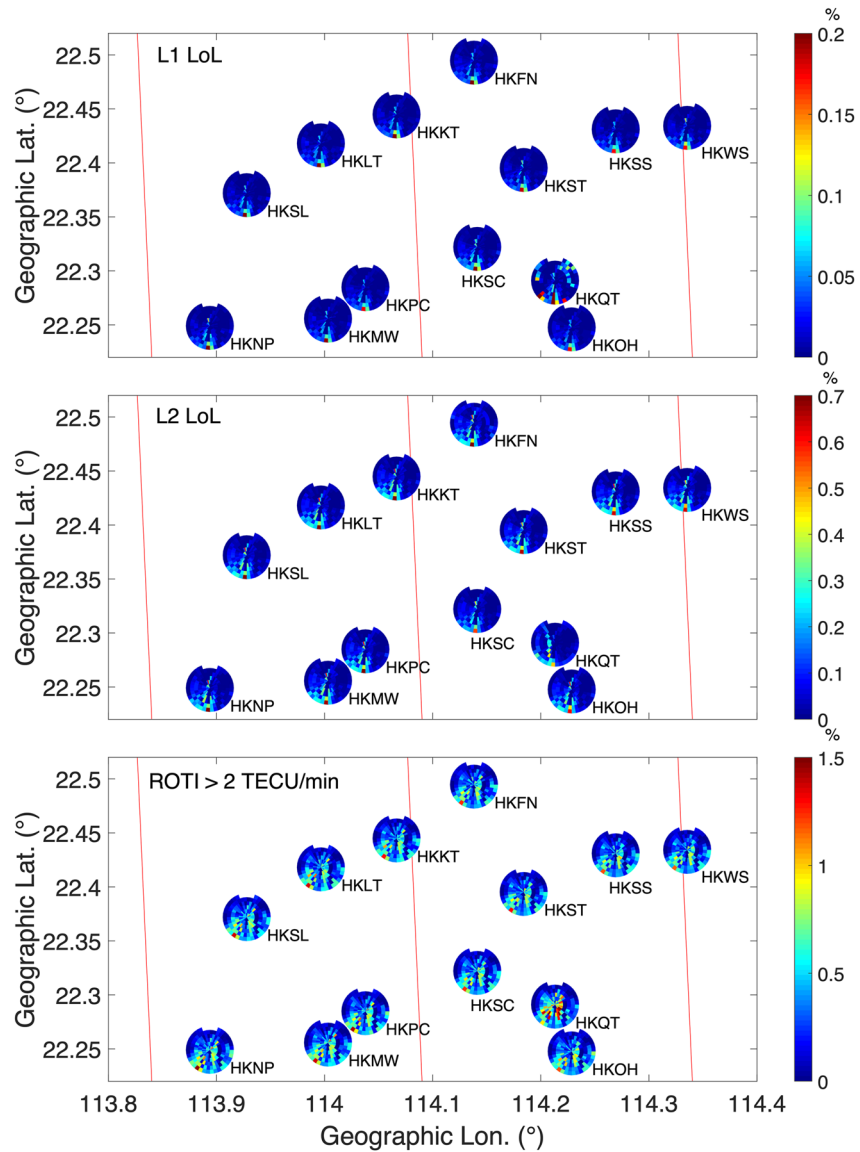
3.2.2. Spatial Distribution of ROTI and LoL

Based on the evolution progress of ionospheric irregularities in the equatorial and low latitude, it is considered that low-latitude ionospheric irregularities typically exist from geomagnetic equator to the EIA region (Kintner et al., 2007), and distribute along the geomagnetic field (field-aligned irregularities structures) (Otsuka et al., 2002). The GNSS stations used in this study are located in a very narrow zone of geographic latitude 22.2°–22.6°N that is near the northern EIA crest in this longitude (J. Liu et al., 2020). So the spatial distribution of the ionospheric irregularities should be obvious in this region.

The elevation and azimuth distributions of LoL occurrence and ROTI >2 TECU/min percentage averaged over all the 5 years 2012–2016 for every station are presented in Figure 10. Results from each station are given separately in a circular chart, where the center stands for the location of the receiver, and the edge of the circle corresponds to an elevation angle of 30°. The red lines in the figure represent the geomagnetic field lines in this region, the declination is about −2°. Each cell in the radial direction in the figure represents 10° of elevation, and each cell in the angular direction represents 10° of azimuth. It can be noticed that the spatial distribution based on the same kind of scintillation-related parameters from different receivers is generally consistent. Lower elevation angles correspond to higher LoL and strong irregularities percentage, with
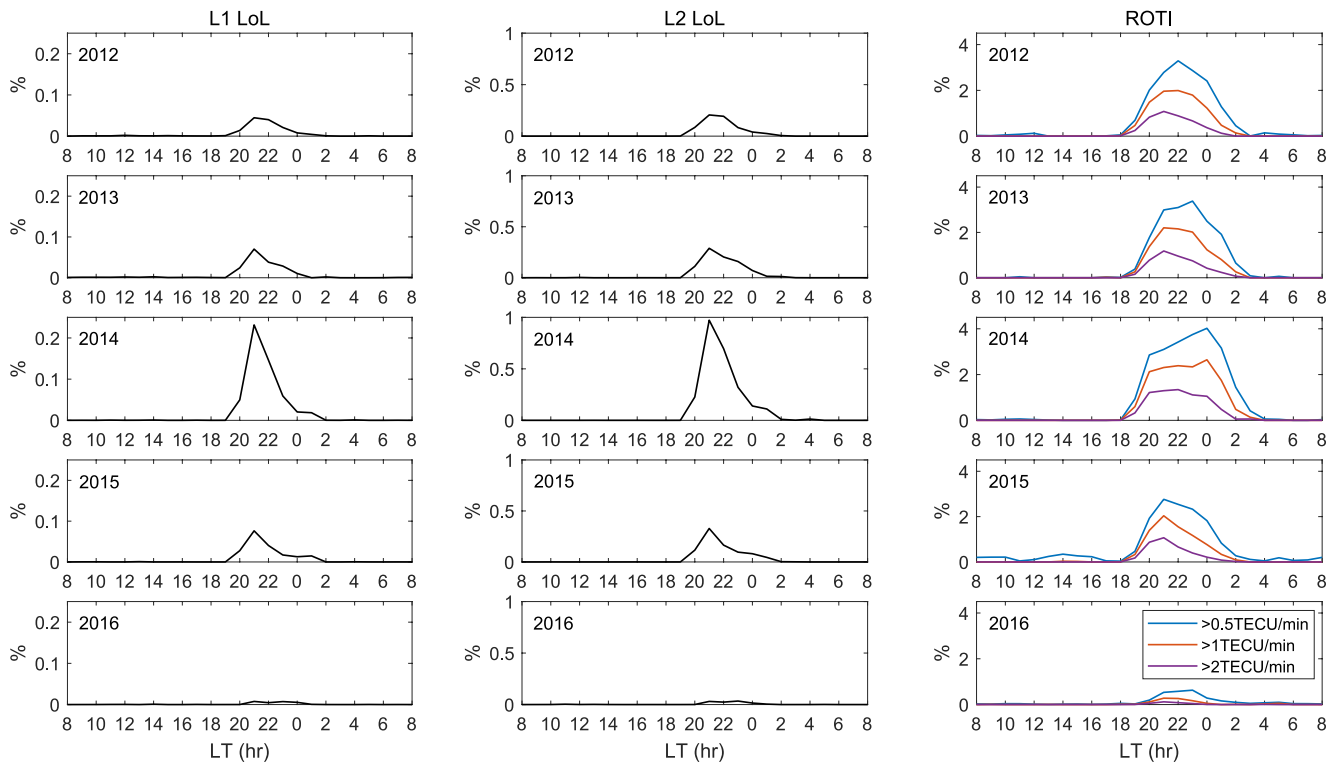

Figure 9. Local time variations of loss of lock occurrence in L1, L2, and the occurrence of ROTI with three levels during 2012–2016, all the data are averaged over 12 stations (excluding HKCL and HKQT).

Figure 10. Spatial distribution of (top) loss of lock (LoL) occurrence in L1, (middle) LoL occurrence in L2 and (bottom) the occurrence of ROTI >2 TECU/min observed from each station, averaged over 5 years (2012–2016). In each circular chart, each cell in the radial direction represents 10° of elevation, and each cell in the angular direction represents 10° of azimuth. The lower bound of elevation, corresponding to the edge of each circular chart, is 30°. Red solid lines represent the geomagnetic field lines in this region.

the highest values between elevations 30° and 40°. This is because the signals of lower elevation angles propagate longer paths of the ionosphere and are more probable to be affected by the ionospheric irregularities. As for azimuthal distribution, both LoL in L1 and L2 occur mainly between azimuths 160° and 240°. This distribution presents that the strong ionospheric irregularities mainly exist in the south side of the observation sites. However, the spatial distribution of ROTI deviates a little from that of LoL. Compared to the LoL, the elevation and azimuth distribution of ROTI is more scattered. The LoL occurrences reach maximum between azimuths 180° and 190°, while ROTI occurrence reaches maximum between 210° and 220° and its elevation distribution is much wider than that of LoL in L1 and L2. As a comparison, the spatial distribution of LoL and ROTI from HKQT station is also plotted in Figure 10. It can be seen that the distribution from this station is a little different with that from other 12 stations. It illustrates that the results from different receivers exist some uncertainties, so, it should be careful when the ROTI and LoL data from single receiver are used to indicate their spatial distribution. Where available, it had better to conduct the cross-data testing. From the spatial distribution of LoL and ROTI, it
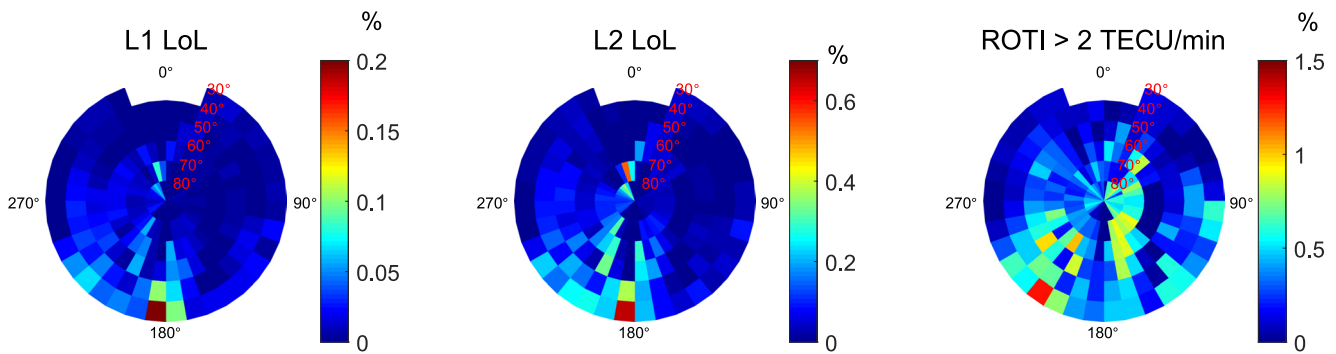
Figure 11. Spatial distribution of (left) loss of lock (LoL) occurrence in L1, (middle) LoL occurrence in L2 and (right) the occurrence of ROTI >2 TECU/min, averaged over 12 stations (excluding HKCL and HKQT) and 5 years 2012–2016.

is found that the most direction of the ionospheric irregularities is south-by-west that is not along the line of the geomagnetic field in this region.

In view of the very similar spatial distribution of the same kind of ionospheric scintillation related parameters from every station, in order to show the spatial distribution of LoL and ROTI clearly, the spatial distribution of LoL (L1 and L2) and ROTI averaged from 12 stations is provided in Figure 11. On the whole, the spatial distribution LoL in L1 and L2 is very similar and the spatial direction is more concentrated than that in ROTI. The spatial distribution of ROTI is more scattered than that of LoL. This difference of the spatial distribution between LoL and ROTI will be discussed in the discussion section too.

3.3. Correlation Between ROTI and LoL Occurrence

In regard to the diurnal and seasonal variation, LoL and ROTI occurrence demonstrate overall consistency, yet the difference between these two parameters should be highlighted. ROTI is a derived quantity based on the temporal variation of TEC in a certain continuous time interval. Although its value is affected by the GNSS satellite orbit or the IPP trajectory, its value can reflect the status of the ionospheric irregularities statistically (Basu et al., 1999). Comparatively, LoL event is essentially an abnormal phenomenon in GNSS performing process, its occurrence is much related to strong ionospheric irregularities condition. It should be noted that when LoL event in L1 or L2 occurs, the TEC cannot be calculated. So, the ROTI cannot be obtained at the epoch when LoL event occurs. Nevertheless, considering the connections across different scales of ionospheric irregularities, intense scintillation-induced abnormal GNSS performing events (represented by LoL occurrence) is supposed to be correlated to the intensity of ionospheric fluctuation (represented by ROTI) statistically.

The results shown in Figures 6, 8 and 9 have proven the data reliability and the correlation between ionospheric irregularities (represented by ROTI) and scintillation effect (represented by LoL). However, these figures present ROTI and LoL in separate panels, so the relationship of the LoL occurrence and ROTI percentage is not sufficiently clear. To reflect the correlation between ROTI and LoL more directly, Figure 12 gives the relationship of the LoL occurrence percentage in L1 and L2 with the corresponding ROTI ranges (interval step is 0.5 TECU/min) for 12 stations. The results are from the averaged data of all the 5 years for each station. In order to show the confidence level of the statistical results, total numbers of measurement in each ROTI range are also shown (red line). It should be noted that for a single receiver, ROTI cannot be calculated when LoL in L1 or L2 occurs. So instead of calculating the LoL occurrence over the 5-min interval of ROTI, LoL occurrence is calculated over the two 30-s intervals which immediately precede and follow the 5-min interval of the ROTI calculating. ROTI greater than 7 TECU/min is not further scaled, so the rightmost data point in each panel includes the total number of measurement for ROTI >7 TECU/min, that is, the number of measurements in the rightmost point is the accumulated measurement numbers for ROTI >7 TECU/min. As the figure indicates, with the increase of ROTI value, LoL occurrence percentage of each station gradually increase in general, but there are some small discrepancies among the stations. These discrepancies intensify as ROTI larger than 5 TECU/min. There are also some instances in some stations where LoL occurrence percentage significantly falls even when ROTI increases, which may be partially related to the decrease of measurement number when ROTI is high. To mitigate the influence of receivers' individual difference, the data of 12 stations in this small region can be summed up to describe the relationship between ROTI and LoL, as in Figure 13. Figure 13a shows the relationship between the LoL occurrence with the corresponding interval of ROTI value that
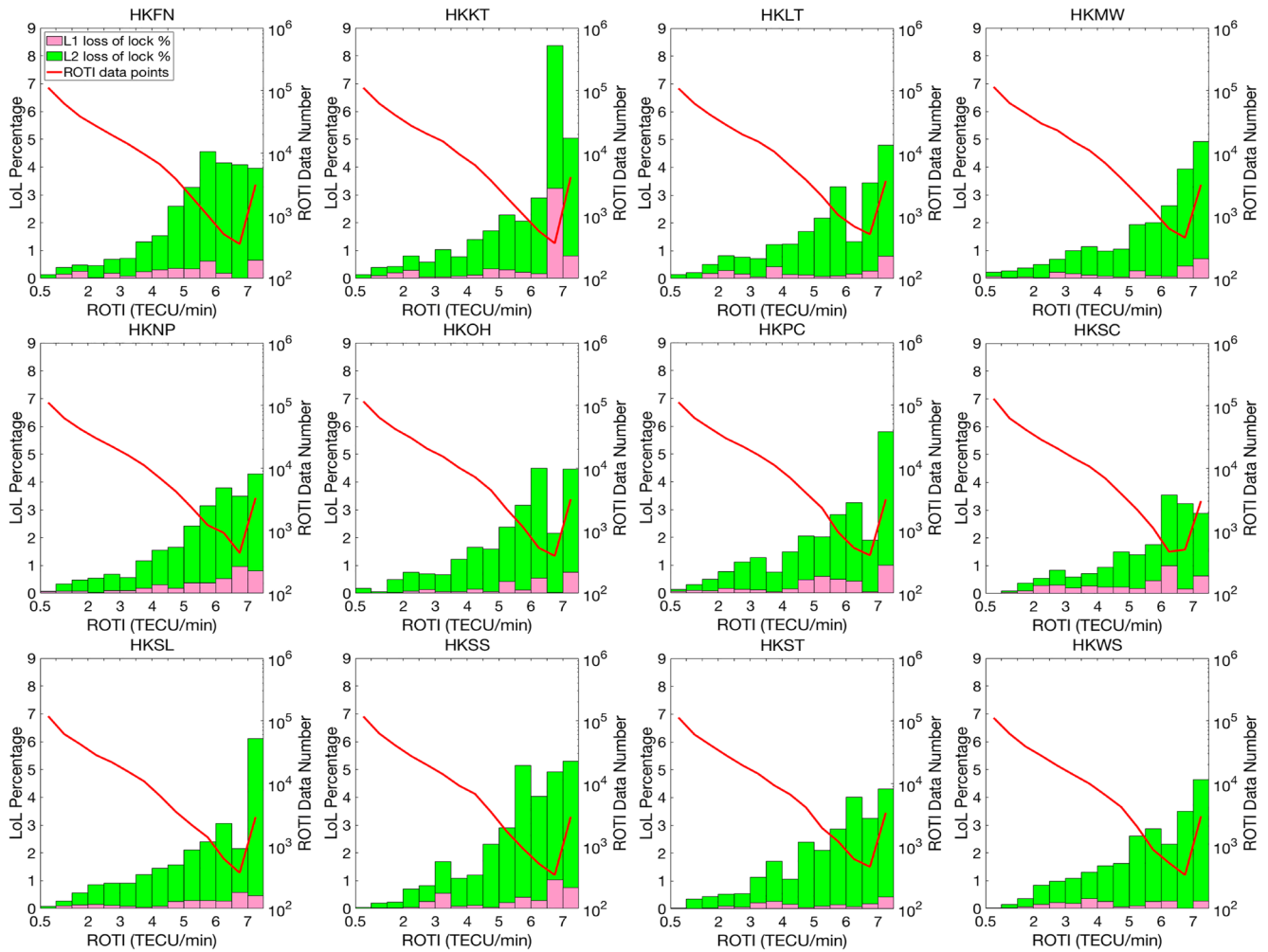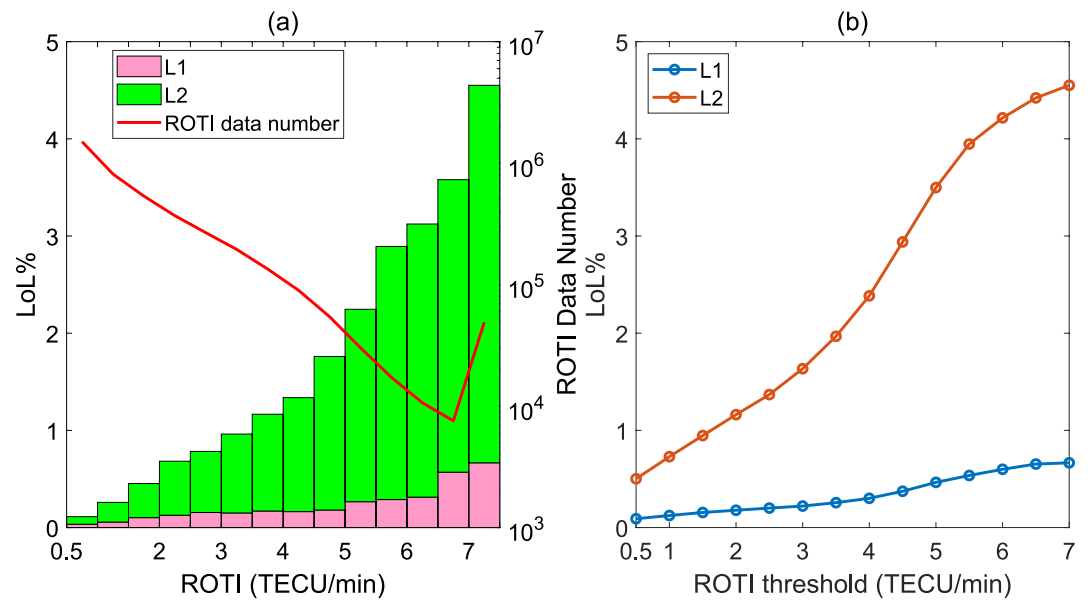
Figure 12. Bar plot of the loss of lock percentage in L1 (pink) and L2 (green) signal in given ROTI ranges (from 0.5 to 1.0 TECU/min to 6.5–7.0 TECU/min, and >7.0 TECU/min) of 12 stations during 2012–2016. The red line denotes the number of ROTI data points in each ROTI range.

is obtained by average of all the data of 12 stations. Figure 13b shows the relationship between the LoL occurrence and the ROTI occurrence for the ROTI larger than certain value with the same data in Figure 13a. In this figure, it can be seen that the LoL occurrence percentage of L1 and L2 is positively correlated with ROTI, and the LoL occurrence percentage in L1 and L2 when the ROTI >5 TECU/min is 0.5% and 3.5%, respectively. This indicates that multi-station network can restrain the discrepancies of derived data due to individual difference of receiver.

4. Discussion

In the previous section, it has been shown that the seasonal, diurnal, azimuthal and elevational variations of ROTI and LoL generally accord with our knowledge of the variation of the ionospheric irregularities or scintillation in China low latitude region. ROTI and LoL are basically correlated, and results from multiple receivers present better ROTI-LoL occurrence correlation than that from single receiver, proving the advantage of a small regional GNSS network over single station observation.

In practice, apart from ionospheric irregularities, some ionospheric unrelated factors can also bring about the LoL event and large ROTI value in GNSS measurements. To obtain reliable results in irregularities and scintillation studies, these abnormal LoL events and ROTI data caused by factors unrelated to ionospheric irregularities should be eliminated. This study presents two methods to detect the data of some typical abnormal events, one is based on cross examination among multiple stations, and the other is based on a priori knowledge of the morphology of the ionospheric irregularities in the low latitude region of China. The former method requires multi-station

Figure 13. Correlation between loss of lock percentage and ROTI, averaged over 12 stations. (a) The labels and ROTI ranges are the same as Figure 12. Note that the ROTI data number in this figure is the sum of 12 stations. (b) Similar to (a), but ROTI ranges are chosen as greater than a certain threshold (from >0.5 TECU/min, >1.0 TECU/min to >7.0 TECU/min).

data in a small region, and the latter requires long-term observation data. Besides the elimination of abnormal data, the determination of the ROTI threshold is another aspect that can affect the results of the irregularities studies. With the advance of manufacturing technique and data processing algorithms, modern GNSS receivers are able to provide data with higher sampling rate, more precision and stability than before. As ROTI values depend on the sampling rate of the observation, and the ROTI from different sampling rates reflect different scales of ionospheric irregularity (Basu et al., 1999), it is necessary to determine the boundary value between the ionospheric background fluctuation component and irregularity-related components, that is, the ROTI threshold. In this study, a priori temporal distribution of ionospheric irregularities in this region is used to determine the threshold of ROTI calculated from TEC data with 5-s sampling rate via statistical analysis.

Although both ROTI and LoL can be used to describe the primary morphology of ionospheric scintillation or irregularities and display similar features in temporal and spatial distribution, there are noteworthy discrepancies in detail. For seasonal variation, LoL rarely occurs outside equinox months, and for local time variation, LoL occurs in a narrower time range than ROTI. This can be explained by the different causes of LoL and ROTI. LoL is an abnormal phenomenon of GNSS signals, its occurrence mainly depends on intense ionospheric irregularities along the signal path. Considering its cause, LoL thus statistically mainly occurs under strong irregularities conditions, so the distributional features of LoL reflect mainly the distribution of strong scintillation or strong irregularities. In contrast, ROTI is derived from 5-min continuous TEC data, which cannot be calculated when LoL occurs. This may be one of the reasons for the difference of temporal distribution between the ROTI and LoL. On the other hand, as Basu et al. (1999) mentioned, the ROTI is more sensitive to the specific scale of the ionospheric irregularities that is determined by the sampling rate of the TEC. For the ROTI calculated using the TEC with 5-s sampling rate in this study, the sensitive scale of the irregularities is about 1 km that can last more hours after midnight. On the whole, the discrepancy in temporal distribution can thus be explained by the fact that LoL and ROTI represent different levels of ionospheric fluctuation in irregularities strength and scale.

Spatial distribution of the LoL and ROTI reveals obvious differences. Their azimuth distributions of the occurrence rate are a little different, and the azimuthal distribution of LoL is more concentrated. According to the spatial distribution of the parameters from different stations, the consistency among the same type of parameter is very good, but the discrepancies between LoL and ROTI are significant. These discrepancies should reflect different effects that ionospheric irregularities pose on the two parameters.

Based on S4 data from 2011 to 2016 at Shenzhen station, M. Zhang et al. (2019) found that local time variations for different scintillation intensity is not same. The local time variation of the intense scintillation condition
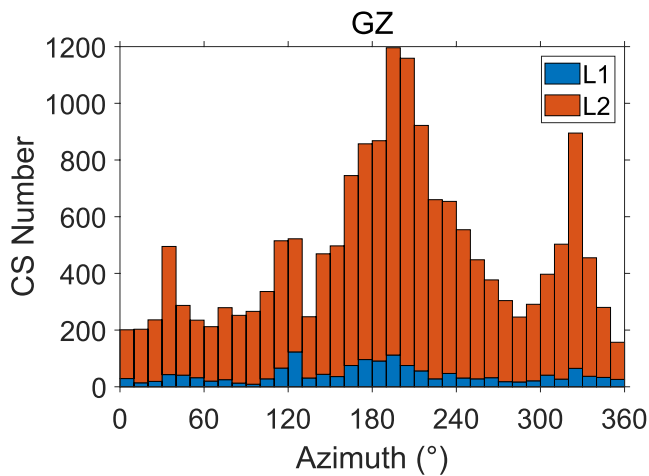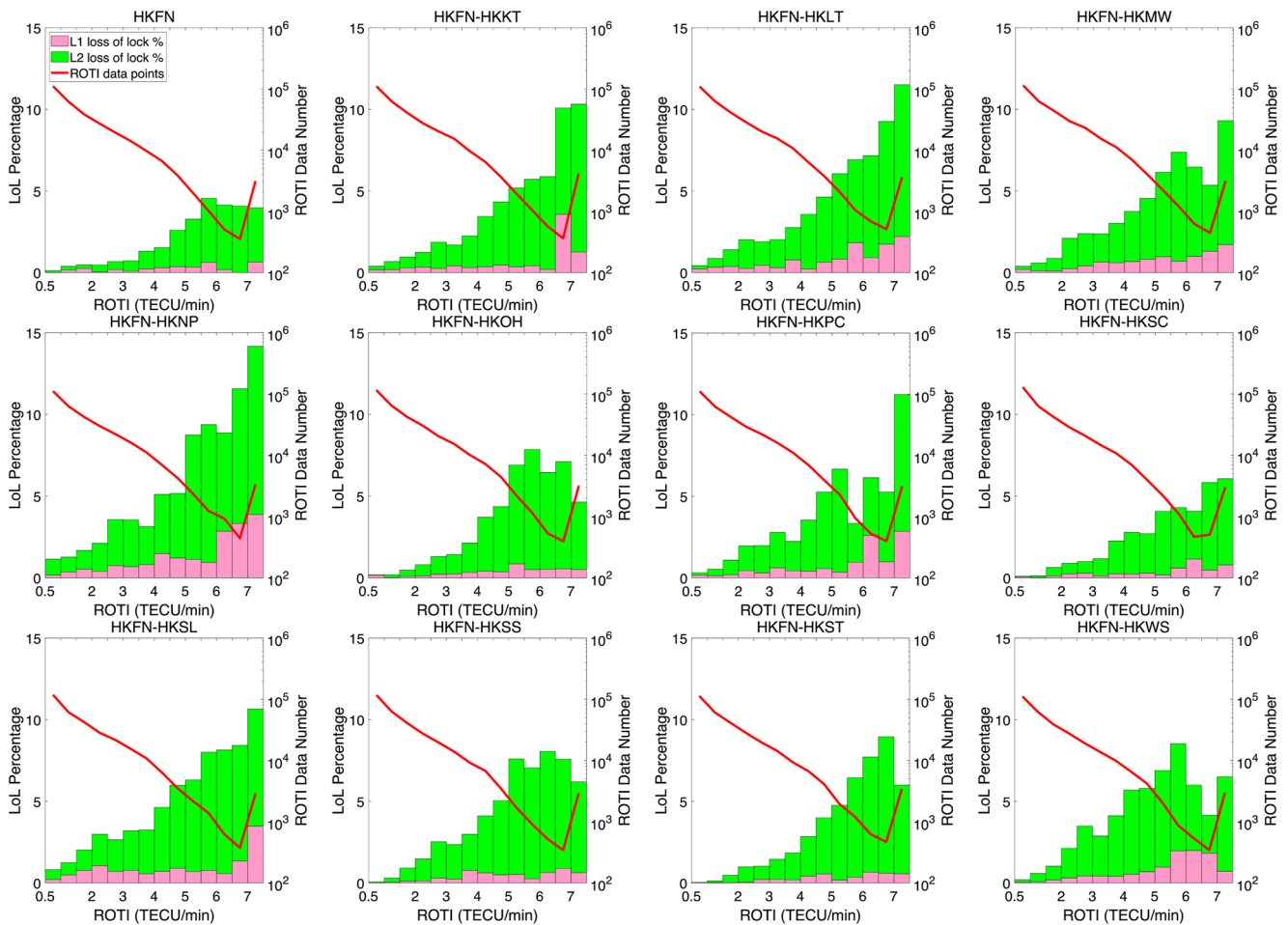
Figure 14. The azimuth distribution of accumulated cycle slip number from 1999 to 2006 in L1 and L2 at Guangzhou station.

(S4 > 0.6) is very consistent with LoL occurrence that the maximum generally occurs at around 09:00 LT and the intense scintillation seldom occurs after midnight. The local time variation of the weak scintillation (0.2 < S4 < 0.4) is similar with the ROTI variation that, the maximum generally occurs before midnight, and the occurrence can extend to around 02:00 LT or so. This shows that the LoL mainly reflects the condition of the intense scintillation or strong irregularities. In the meantime, it fails to reflect the weak or even moderate scintillation or irregularities condition. As for ROTI, because the ROTI cannot be obtained when LoL occurs, the ROTI cannot indicate the condition of the intense scintillation or strong irregularities in spatial and temporal distribution. In addition, the ROTI depends on the particular viewing geometry for each satellite and the relative velocity between the ionospheric penetration point (IPP) and the drifting irregularities (Basu et al., 1999; Carrano et al., 2019). These factors may be responsible for the difference of azimuth distribution between ROTI and LoL, also for the more spatially scattered distribution of ROTI showed in Figures 10 and 11.

Although there is detailed difference in azimuthal distribution between these two parameters, we can notice that the azimuthal maxima of both parameters occur in the south-by-west direction. Considering the generation and evolution process of the ionospheric irregularities in the equatorial and low-latitude, a maximum in the south is reasonable. But a maximum in the south-by-west direction mismatches our understanding of the evolution process of low-latitude irregularities. When irregularities evolve toward higher latitudes, they move gradually along the magnetic field lines that is so-called the ionospheric field-aligned irregularities. Since the magnetic declination angle in this area is negative, field-aligned irregularities should have distributed along the southeast-northwest direction. According to this understanding, statistically the maximum effect of ionospheric irregularities should occur in the south-by-east direction, instead of south-by-west as shown in Figure 11. The data coverage in Figure 11 is 5 years from 2012 to 2016. As ionospheric irregularities has significant day-to-day, seasonal and local time variation, the spatial distribution pattern in Figure 11 may be deviated by some solitary strong irregularities events. To determine this direction distribution of the ionospheric irregularities further, the CS occurrence number collected from Guangzhou GNSS station (23.2°N, 113.3°E) near the SatRef GNSS network is used to show the spatial distribution of CS events in this region. It should note that the CS detection depends on the algorithm and the threshold choice of slip (Blewitt, 1990; Collin & Warnant, 1995; Li et al., 2022). The CS detection method here is from Teunissen (1990) and the sampling rate is 30-s Figure 14 shows the azimuth distribution of accumulated CS occurrence number in L1 and L2 at Guangzhou station from 1999 to 2006. It can be seen that the azimuth of maximum occurrence of CS is also in the south-by-west direction (190–200°). In addition, Cheng et al. (2018) studied azimuthal distribution of scintillation based on S4, ROTI and CS data from Hong Kong and Nanning, China, and their distributional features are consistent with our results. Through the statistical results of different data in the same period and different scintillation-related parameters in different periods, we consider that the azimuthal distribution characteristic in Figure 11 is convincible. But it seems a little different from expected distribution of low-latitude field-aligned irregularities. Huang et al. (2010) found that during solar maximum, equatorial plasma bubbles generally drift eastward, and in most cases the zonal velocity of the bubble structure is faster than the ambient plasma drift. This might explain the south-by-west orientation of LoL and ROTI parameters. If the zonal drift velocity component of the irregularity structure is eastward, considering the northward drift along magnetic field lines, the resultant velocity of the irregularity should be northeastward, which results in a southwest-northeast orientation of the irregularity.

A problem of the previous correlation in Figure 12 is that, for a single receiver, since ROTI cannot be calculated when LoL occurs, the temporal coverages of LoL and ROTI do not overlap. As a makeshift, ROTI and LoL are calculated over different intervals. LoL is collected over two 30-s intervals which immediately precede and follow the 5-min interval of ROTI calculating, but the interval length of 30 s is arbitrary, and results may be slightly different if another interval length is chosen. This flaw can be partly fixed through cross-correlation between different stations. As LoL is a random phenomenon, when one receiver experiences LoL, it is possible that its neighboring receivers do not lose track and can provide ROTI. Figure 15 presents the correlation of LoL from HKFN and the ROTI from the other receivers with same 5-min interval during 2012–2016. It can be seen that the correlation between different receivers inside a small regional network is generally better than the self-correlation

Figure 15. Correlation between loss of lock (LoL) percentage from HKFN and ROTI from the other 11 stations during 2012–2016. Self-correlation of LoL percentage and ROTI at HKFN station in the upper left "HKFN" panel (same as the "HKFN" panel in Figure 12) is also shown.

of a single receiver. Note that in Figure 15, LoL in HKFN is calculated over the same 5-min interval as ROTI calculated in other 11 stations, not the two 30-s intervals as in Figure 12 (except for HKFN station).

Apart from LoL and ROTI, traditional S4 index is another alternative for cross-correlation analysis. Figure 16 shows the correlation of the LoL occurrence percentage in L1 and L2 signal of 12 GNSS stations with the different S4 strength interval observed at Shenzhen station in 2014. In Figure 16, all the stations exhibit good positive correlation between S4 and LoL occurrence. Unlike that in Figure 12, there is no significant discrepancy among the 12 panels. Note that when S4 is close to 1, the LoL percentage can be as high as 30% or more, which is different from the previous case of using ROTI as the indicator of irregularities, where LoL% remains below 5% even when ROTI exceeds 7 TECU/min. As mentioned above, LoL and ROTI represent the different strength irregularities, LoL for intense scintillation or strong irregularities condition and ROTI mainly for weak or moderate scintillation or irregularities condition. That may be the main reason for the lower percentage of LoL occurrence in Figures 12 and 13. These results indicate that the traditional single receiver-based ROTI is still capable of reflecting the strong irregularities to some extent, but it is recommended to improve data quality through averaging and cross-correlation among multiple stations in a regional network whenever possible.

5. Conclusions

Ionospheric scintillation-related parameters derived from GNSS observations are an important data source for ionospheric scintillation and irregularities studies. However, there are certain limitations of these data in reflecting ionospheric scintillation and irregularities, and clearing these limitations is very important for us to understand the results based on these data. In this paper, ROTI and LoL from a GNSS network with high spatial
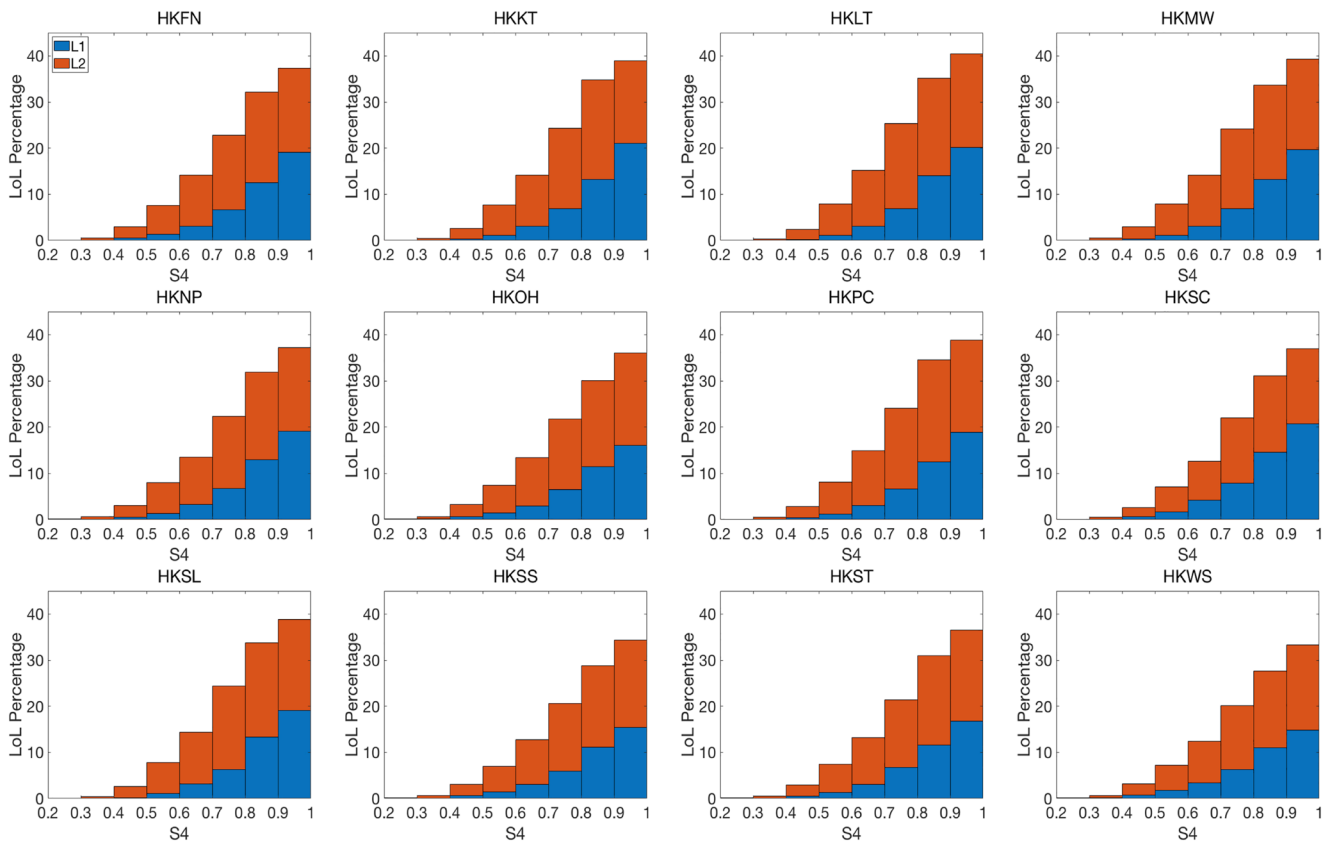
Figure 16. Correlation between the loss of lock percentage of the 12 SatRef stations and S4 from Shenzhen (SZ) station in 2014.

distribution density in the low latitude region of China are used to revisit the variation of the ionospheric irregularities, especially to show the consistence and difference of the ionospheric irregularities represented in ROTI and LoL parameters. The main conclusions are follows:

1. Via a priori knowledge of scintillation and irregularities temporal variation in this area and comparison among stations, a method to determine the threshold ROTI for discriminating quiet and disturbed conditions is provided. Through statistical analysis of 5-s sampling rate ROTI, the threshold of ROTI is determined as 0.5 TECU/min.
2. The same parameter from different stations shows good consistency when abnormal data are eliminated. The local time and seasonal distributions of ROTI and LoL are generally consistent with the morphology of scintillation and irregularities in this area, but there are discrepancies in detail. For local time variation, ROTI is more temporally extensive than LoL. The maximum occurrence of LoL is at around 21:00 LT. The maximum occurrence of ROTI is not significant, it is between 20:00 LT and 23:00 LT.
3. For spatial distribution, the same parameter from different receiver is very consistent. But there is obvious difference in spatial distribution in LoL and ROTI. LoL is more spatially concentrated than ROTI. The azimuth range of maximum occurrence is 180–190° for LoL and 210–220° for ROTI.
4. Correlation between ROTI and LoL from single station is high for small ROTI, but declines when ROTI >5 TECU/min. However, the correlation improves greatly when data are averaged among all the stations.
5. LoL tends to occur during intense scintillation or strong irregularities when ROTI is unavailable, hence ROTI has limitation reflecting the morphology of strong irregularities, our result shows that this limitation can be partially mitigated by using multiple stations in a small regional network.

Data Availability Statement

The GNSS data are from the Hong Kong Satellite Positioning Reference Station Network (SatRef) (https://www.geodetic.gov.hk/en/rinex/downv.aspx). The S4 data are from the Chinese Meridian Project (data2.meridianproject.ac.cn).

References

Aarons, J. (1977). Equatorial scintillations: A review. *IEEE Transactions on Antennas and Propagation*, 25(5), 729–736. https://doi.org/10.1109/tap.1977.1141649

Aarons, J. (1982). Global morphology of ionospheric scintillations. *Proceedings of the IEEE*, 70(4), 360–378. https://doi.org/10.1109/PROC.1982.12314

Aarons, J., Mendillo, M., Yantosca, R., & Kudeki, E. (1996). GPS phase fluctuations in the equatorial region during the MISETA 1994 campaign. *Journal of Geophysical Research*, 101(A12), 26851–26862. https://doi.org/10.1029/96ja00981

Abdu, M. A., & Kherani, E. A. (2011). *Coupling processes in the equatorial spread F/plasma bubble irregularity development, Aeronomy of the Earth's Atmosphere and Ionosphere* (pp. 219–238). Springer.

Basu, S., & Basu, S. (1981). Equatorial scintillations—A review. *Journal of Atmospheric and Terrestrial Physics*, 43(5–6), 473–489. https://doi.org/10.1016/0021-9169(81)90110-0

Basu, S., Groves, K. M., Quinn, J. M., & Doherty, P. (1999). A comparison of TEC fluctuations and scintillations at Ascension Island. *Journal of Atmospheric and Solar-Terrestrial Physics*, 61(16), 1219–1226. https://doi.org/10.1016/S1364-6826(99)00052-8

Blewitt, G. (1990). An automatic editing algorithm for GPS data. *Geophysical Research Letters*, 17(3), 199–202. https://doi.org/10.1029/GL017i003p00199

Carrano, C. S., Groves, K. M., & Rino, C. L. (2019). On the relationship between the rate of change of total electron content index (ROTI), irregularity strength (CkL), and the scintillation index (S4). *Journal of Geophysical Research: Space Physics*, 124(3), 2099–2112. https://doi.org/10.1029/2018JA026353

Chen, Z. Y., Gao, Y., & Liu, Z. Z. (2005). Evaluation of solar radio bursts' effect on GPS receiver signal tracking within International GPS Service network. *Radio Science*, 40(3), RS3012. https://doi.org/10.1029/2004rs003066

Cheng, J., Xu, J. S., & Cai, L. (2018). A comparison of statistical features of ionospheric scintillations and cycle slips in the mid-south region of China (in Chinese). *Chinese Journal of Geophysics*, 61(1), 18–29. https://doi.org/10.6038/cjg2018L0065

Cherniak, I, Krankowski, A., & Zakharenkova, I. (2018). ROTI maps: A new IGS ionospheric product characterizing the ionospheric irregularities occurrence. *GPS Solutions*, 22(3), 69. https://doi.org/10.1007/s10291-018-0730-1

Collin, F., & Warnant, R. (1995). Application of the wavelet transform for GPS cycle slip correction and comparison with Kalman filter. *Manuscripta Geodaetica*, 20(3), 161–172.

Damaceno, J. G., Bolmgren, K., Bruno, J., De Franceschi, G., Mitchell, C., & Cafaro, M. (2020). GPS loss of lock statistics over Brazil during the 24th solar cycle. *Advances in Space Research*, 66(2), 219–225. https://doi.org/10.1016/j.asr.2020.03.041

Huang, C.-S., de La Beaujardiere, O., Pfaff, R. F., Retterer, J. M., Roddy, P. A., Hunton, D. E., et al. (2010). Zonal drift of plasma particles inside equatorial plasma bubbles and its relation to the zonal drift of the bubble structure. *Journal of Geophysical Research*, 115, A07316. https://doi.org/10.1029/2010JA015324

Jacobsen, K. S. (2014). The impact of different sampling rates and calculations time intervals on ROTI values. *Journal of Space Weather Space Climate*, 4, A33. https://doi.org/10.1051/swsc/2014031

Kintner, P. M., Ledvina, B. M., & De Paula, E. R. (2007). GPS and ionospheric scintillations. *Space Weather*, 5(9). https://doi.org/10.1029/2006sw000260

Li, W., Song, S., & Jin, X. (2022). Ionospheric scintillation monitoring with ROTI from geodetic receiver: Limitations and performance evaluation. *Radio Science*, 57(5), e2021RS007420. https://doi.org/10.1029/2021RS007420

Liu, J., Zhang, D., Mo, X., Xiong, C., Hao, Y., & Xiao, Z. (2020). Morphological differences of the northern equatorial ionization anomaly between the eastern Asian and American sectors. *Journal of Geophysical Research: Space Physics*, 125(3), e2019JA027506. https://doi.org/10.1029/2019ja027506

Liu, Y., Fu, L., Wang, J., & Zhang, C. (2017). Study of GNSS loss of lock characteristics under ionosphere scintillation with GNSS data at Weipa (Australia) during solar maximum phase. *Sensors*, 17(10), 2205. https://doi.org/10.3390/s17102205

Liu, Z., Yang, Z., Xu, D., & Morton, Y. J. (2019). On inconsistent ROTI derived from multiconstellation GNSS measurements of globally distributed GNSS receivers for ionospheric irregularities characterization. *Radio Science*, 54(3), 215–232. https://doi.org/10.1029/2018RS006596

Olwendo, J. O., Cilliers, P., Weimin, Z., Ming, O., & Yu, X. (2018). Validation of ROTI for ionospheric amplitude scintillation measurements in a low-latitude region over Africa. *Radio Science*, 53(7), 876–887. https://doi.org/10.1029/2017RS006391

Otsuka, Y., Shiokawa, K., Ogawa, T., & Wilkinson, P. (2002). Geomagnetic conjugate observations of equatorial airglow depletions. *Geophysical Research Letters*, 29(15), 1753–43-4. https://doi.org/10.1029/2002gl015347

Pi, X., Mannucci, A., Lindqwister, U., & Ho, C. (1997). Monitoring of global ionospheric irregularities using the worldwide GPS network. *Geophysical Research Letters*, 24(18), 2283–2286. https://doi.org/10.1029/97GL02273

Rino, C. L. (1979a). A power law phase screen model for ionospheric scintillation: 1. Weak scatter. *Radio Science*, 14(6), 1135–1145. https://doi.org/10.1029/rs014i006p01135

Rino, C. L. (1979b). A power law phase screen model for ionospheric scintillation: 2. Strong scatter. *Radio Science*, 14(6), 1147–1155. https://doi.org/10.1029/rs014i006p01147

Rino, C. L., & Fremouw, E. J. (1977). The angle dependence of singly scattered wave fields. *Journal of Atmospheric and Terrestrial Physics*, 39(8), 859–868. https://doi.org/10.1016/0021-9169(77)90166-0

Sultan, P. J. (1996). Linear theory and modeling of the Rayleigh-Taylor instability leading to the occurrence of equatorial spread F. *Journal of Geophysical Research*, 101(A12), 26875–26891. https://doi.org/10.1029/96ja00682

Teunissen, P. J. G. (1990). Quality control in integrated navigation systems. *IEEE Aerospace and Electronic Systems Magazine*, 5(7), 35–41. https://doi.org/10.1109/62.134219

Tsunoda, R. T. (1985). Control of the seasonal and longitudinal occurrence of equatorial scintillations by the longitudinal gradient in the integrate E region Pedersen conductivity. *Journal of Geophysical Research*, 90(A1), 447–456. https://doi.org/10.1029/JA090iA01p00447

Van Dierendonck, A. J., Klobuchar, J., & Hua, Q. (1993). Ionospheric scintillation monitoring using commercial single frequency C/A code receivers. In *Paper presented at the 6th International Technical Meeting of the Satellite Division of The Institute of Navigation (ION GPS 1993), Salt Lake City, Utah, 22–24 September*.

Van Velthoven, P. F. J. (1990). *Medium scale irregularities in the ionospheric electron content* (PhD-Thesis). Universiteit Eindhoven.

Wanninger, L. (1993). Ionospheric monitoring using IGS data. In *Proceedings of the 1993 Berne IGS Workshop, International GPS Service for Geodynamics, Berne, Switzerland, March 25–26*.

Xiong, C., Stolle, C., & Park, J. (2018). Climatology of GPS signal loss observed by Swarm satellites. *Annales Geophysicae*, 36(2), 679–693. https://doi.org/10.5194/angeo-36-679-2018

Yang, Z., & Liu, Z. Z. (2016). Correlation between ROTI and ionospheric scintillation indices using Hong Kong low-latitude GPS data. *GPS Solutions*, *20*(4), 815–824. https://doi.org/10.1007/s10291-015-0492-y

Yeh, K. C., & Liu, C. H. (1982). Radio wave scintillations in the ionosphere. *Proceedings of the IEEE*, *70*(4), 324–360. https://doi.org/10.1109/proc.1982.12313

Zhang, D. H., Cai, L., Hao, Y. Q., Xiao, Z., Shi, L. Q., Yang, G. L., & Suo, Y. C. (2010a). Solar cycle variation of the GPS cycle slip occurrence in China low-latitude region. *Space Weather*, *8*(10), S10D10. https://doi.org/10.1029/2010sw000583

Zhang, D. H., Xiao, Z., Feng, M., Hao, Y. Q., Shi, L. Q., Yang, G. L., & Suo, Y. C. (2010b). Temporal dependence of GPS cycle slip related to ionospheric irregularities over China low-latitude region. *Space Weather*, *8*(4), S04D08. https://doi.org/10.1029/2008sw000438

Zhang, D. H., Zhang, W., Li, Q., Shi, L. Q., Hao, Y. Q., & Xiao, Z. (2010c). Accuracy analysis of the GPS instrumental bias estimated from observations in middle and low latitudes. *Annales Geophysicae*, *28*(8), 1571–1580. https://doi.org/10.5194/angeo-28-1571-2010

Zhang, M., Zhang, D. H., Hao, Y. Q., & Xiao, Z. (2019). A statistical study on L-band ionospheric amplitude scintillation in Shenzhen during 2011–2016 (in Chinese). *Science and information technology*, *49*, 1570–1582. https://doi.org/10.1360/SST-2019-0093